Cobalt incorporation in calcite: thermochemistry of $(Ca,Co)CO_3$ solid solutions from density functional theory simulations

JORGE GONZALEZ-LOPEZ,[1] SERGIO E. RUIZ-HERNANDEZ,[2] ANGELES FERNANDEZ-GONZALEZ,[1] AMALIA JIMENEZ,[1] NORA H. DE LEEUW[2] and RICARDO GRAU-CRESPO[3*]

[1] Department of Geology, University of Oviedo, Calle Arias de Velasco s/n, Oviedo 33005, Spain

[2] Department of Chemistry. University College London, 20 Gordon St. London WC1H 0AJ, UK.

[3] Department of Chemistry. University of Reading, Whiteknights

Reading, RG6 6AD, UK. Email: r.grau-crespo@reading.ac.uk

(Submitted on 24 March, 201; revised version on 30 June 2014)

Abstract– The incorporation of cobalt in mixed metal carbonates is a possible route to the immobilization of this toxic element in the environment. However, the thermodynamics of $(Ca,Co)CO_3$ solid solutions are still unclear due to conflicting data from experiment and from the observation of natural ocurrences. We report here the results of a computer simulation study of the mixing of calcite ($CaCO_3$) and spherocobaltite ($CoCO_3$), using density functional theory calculations. Our simulations suggest that previously proposed thermodynamic models, based only on observed compositions, significantly overestimate the solubility between the two solids and therefore underestimate the extension of the miscibility gap under ambient conditions. The enthalpy of mixing of the disordered solid solution is strongly positive and moderately asymmetric: calcium incorporation in spherocobaltite is more endothermic than cobalt incorporation in calcite. Ordering of the impurities in (0001) layers is energetically favourable with respect to the disordered solid solution at low temperatures and intermediate compositions, but the ordered phase is still unstable to demixing. We calculate the solvus and spinodal lines in the phase diagram using a sub-regular solution model, and conclude that many $Ca_{1-x}Co_xCO_3$ mineral solid solutions (with observed compositions of up to x=0.027, and above x=0.93) are metastable with respect to phase separation. We also calculate solid/aqueous distribution coefficients to evaluate the effect of the strong non-ideality of mixing on the equilibrium with aqueous solution, showing that the thermodynamically-driven incorporation of cobalt in calcite (and of calcium in spherocobaltite) is always very low, regardless of the Co/Ca ratio of the aqueous environment.

1. INTRODUCTION

Cobalt is a trace element in the Earth's crust, accounting for only 0.0025% of its total weight (Smith and Carson, 1981). As the main constituent of vitamine B12, it is an essential element in animal and human diets. However, cobalt is also a toxic metal and has been considered as a possible carcinogen by the International Agency for Research on Cancer (IARC, 1991). Despite the low amounts of cobalt in the Earth's crust, some areas are enriched in this metal due to both natural and anthropogenic factors (Barceloux, 1999). Cobalt is often brought to the surface of the Earth as a product of mining, and it can accumulate in soils or groundwater. Furthermore, cobalt enters the environment from waste waters and solids as a result of other human activities, including the use and/or waste of Co-alloyed steels, Co-containing fertilizers, pigments and Co-Li batteries. In addition to the natural isotope (^{59}Co), cobalt can also exist as radioactive isotopes, which are important in medicine, nuclear energy and quality control of materials, but when released into the environment they can be dangerous to human health (the half-lives for radioactive decay of ^{58}Co and ^{60}Co are 71 days and 5.27 years, respectively) (ATSDR, 2004). The ions typically forming minerals are Co^{2+} and Co^{3+}, where Co^{2+} is the more soluble (Kim et al., 2006) and therefore its mobility in natural water is higher.

In the presence of CO_3^{2-} ions in solution, Co^{2+} cations can in principle be immobilized in the form of carbonate precipitates. The pure cobalt carbonate, the rare mineral spherocobaltite ($CoCO_3$) is known to exist, but it only forms under extreme hydrothermal conditions (Anthony et al., 2003). Alternatively, cobalt could be incorporated in mixed carbonates, for example, substituting calcium in calcite ($CaCO_3$). The substitution of calcium by other metals in the calcite structure is a well-known and ubiquitous phenomenon (Davis et al., 2000; Lorens, 1981; Meyer, 1984). The impurity composition of calcite crystals often follows closely the composition of the solution from wich the material precipitates (Veizer, 1983). There is therefore considerable interest in using naturally-abundant calcite to confine enviromental pollutants such as manganese, barium, cadmium, and chromium (Katsikopoulos et al., 2008b, 2009; Prieto et al., 1997; Sánchez-Pastor et al., 2011; Wang et al., 2011), and, in principle, the same mechanism could be useful for cobalt immobilization.

Unfortunately, the thermodynamics of cobalt incorporation in calcium carbonate polymorphs are not well understood, and only a handful of studies have dealt with the topic. Glynn (2000) has collected data on natural abundances of $Co_xCa_{1-x}CO_3$ (as well as of many other mixed carbonate minerals), observing that up to 2.7 mol% of Co is incorporated in the calcite mineral, while up to 7 mol% of Ca is incorporated in spherocobaltite. From these data, Glynn proposed parametrizations for the excess free energies of mixing between the two carbonates, using the regular solution model (Hildebrand, 1936; Prieto, 2009) for each end of the solution, and assuming that the maximum amount of impurity in natural samples corresponds to the thermodynamic limit of miscibility (at T=323 K). While still useful as an initial approximation to compare the mixing thermodynamics within a large family of minerals, this approach for the derivation of thermodynamic parameters has some severe limitations. First, equilibrium mixing can occur at *any* composition outside the miscibility gap, and therefore observed impurity levels can be well below the miscibility limit. For example, the composition of the solid solution can be determined by aqueous-solid equilibrium during precipitation, and therefore

by the composition of the aqueous solution. Second, mineral solid solutions often form out of equilibrium, in a range of compositions that is metastable with respect to phase separation into the end members. Glynn's approach would overestimate the excess free energies in the former case, while it would understimate them in the latter, and the discrepancies can be considerable, as we will discuss here. One obvious problem of that approach in the case of the $Co_xCa_{1-x}CO_3$ solid solution, is that it predicts that Co substitution in $CaCO_3$ is more endothermic than Ca substitution in $CoCO_3$. Instead, it is generally observed that entering a large cation in a small cation site ($r[Ca^{2+}]$=1.00 Å; $r[Co^{2+}]$=0.74 Å in 6-fold coordination (Shannon, 1976)) is energetically more expensive than the reverse (De Leeuw and Parker, 2000; McLean, 1957).

Katsikopoulos et al. (2008a) experimentally studied the co-crystallization of Co(II) with calcite under conditions similar to those at the Earth's surface. They confirmed that the Co end-member, spherocobaltite, does not precipitate directly from aqueous solution under these conditions. At high concentrations of Co(II) in solution, the precipitate always contains a Co-rich low-crystallinity phase, which could not be identified unambiguously. In the direct precipitation experiments, from highly supersaturated solutions, the maximum amount of Co in the precipitated calcite-structured phase was 33 mol%. In the case of crystals grown in gel at a lower supersaturation, the maximum Co content was 16 mol%. Although no calorimetric data could be obtained in this work, due to presence of multiple phases in precipitation, a new thermodynamic mixing model was proposed based on an assumed miscibility gap at T=298 K for compositions $0.16<x<0.95$ (where the lower limit was taken from the gel experiment and the higher limit from the thermodynamic model by Glynn (2000)). The resulting sub-regular model has the correct assymmetry (more Co in calcite than Ca in spherocobaltite), but still has the problem that the thermodynamic parameters are derived from the observed compositional limits, which are not necessarily related to thermodynamic miscibility, as discussed above.

In this work, in order to overcome the difficulties in obtaining reliable thermodynamic parameters for this system, we have employed sophisticated ab initio simulation techniques, based on the density functional theory (DFT) and statistical mechanics, to calculate the mixing enthalpies in the $(Ca,Co)CO_3$ binary system. Atomistic computer simulations, which allow the evaluation of thermodynamic properties without the interference of unknown kinetic factors, have been increasingly used in recent years for the investigation of the thermodynamics of mixing and impurity incorporation in carbonates (Fisler et al., 2000; Noguera et al., 2010; Ruiz-Hernandez et al., 2010; Vinograd et al., 2007). While the thermodynamics of the bulk $CaCO_3$-$CoCO_3$ phase have not been simulated so far, a previous study (Braybrook et al., 2002), using classical interatomic potentials, has examined the incorporation of cobalt in calcite surfaces and the subsequent modification of the calcite crystal morphology. Investigating surface impurities is important for the understanding of carbonate growth and nucleation, because the presence in the reaction medium of some divalent cations, including Co^{2+} but also Fe^{2+}, Mg^{2+}, Ni^{2+}, Zn^{2+} and Cu^{2+}, seem to favour the formation of aragonite over calcite (Wada et al., 1995). In the present work we are more interested in bulk incorporation, which, if achieved, would maximise cobalt immobilization. Therefore we will focus on the thermodynamics of bulk mixed phases.

2. METHODOLOGY

2.1 Representation of the disordered solid solution

The disordered $Ca_{1-x}Co_xCO_3$ solid solutions were represented by a symmetry-adapted ensemble of configurations in a supercell, using the methodology implemented in the SOD (Site Occupancy Disorder) program (Grau-Crespo et al., 2007), which has been employed previously in the simulation of a range of mineral solid solutions, including carbonates (Ruiz-Hernandez et al., 2010; Wang et al., 2011), oxides (Benny et al., 2009; Grau-Crespo et al., 2010) and sulfides (Haider et al., 2012; Seminovski et al., 2012). This program generates the complete configurational space for each composition in a supercell of the structure, before extracting the subspace of symmetrically inequivalent configurations, for which energies and other properties are evaluated. In our case, the simulation cell is a 2×2×1 supercell of the calcite hexagonal unit cell (Fig. 1), and the numbers of inequivalent configurations for each composition are listed in Table 1. The criterion for the equivalence of two configurations is the existence of an isometric transformation that converts one configuration into the other, where the transformations considered are simply the symmetry operators of the *parent* structure (in this case those in the $R\bar{3}c$ space group of calcite, combined with the internal translations in the supercell). Once the configurational spectrum is obtained, it is possible to derive thermodynamical properties using statistical mechanics. In the simplest formulation, the extent of occurrence of one particular configuration in the disordered solid in configurational equilibrium can be described by a Boltzmann-like probability which can be calculated from the energy E_m of the configuration, and its degeneracy Ω_m (the number of times that the configuration is repeated in the complete configurational space):

$$P_m = \frac{\Omega_m}{Z}\exp(-E_m / RT) \quad (1)$$

where m=1,…, M (M is the number of inequivalent configurations), R is the gas constant, and Z is the partition function, that guarantees that the sum of all the probabilities equals 1 and also gives access to the calculation of configurational free energies and entropies. It is possible in this way to obtain T-dependent configurational thermodynamic functions and equilibrium degrees of disorder (Grau-Crespo et al., 2009; Ruiz-Salvador et al., 2013; Smith et al., 2010). However, in this work we have focused on only two extreme situations: a) the complete order limit, formally $T \to 0$, where only the most stable arrangement of the ions is considered for each composition; and b) the full disorder limit, formally $T \to \infty$, where the probability in equation (1) reduces to:

$$P_m = \frac{\Omega_m}{\sum_m \Omega_m}. \quad (2)$$

The reason we have ignored the intermediate cases of finite-temperature equilibrium is that, as we will show below, the mixing process in this solid solution is very endothermic. The cation distribution in the solid solution, if this is formed at all, is likely to be determined by kinetic factors and be nearly random. The enthalpy in the full-disorder approximation is then:

$$H = \frac{\sum_m \Omega_m H_m}{\sum_m \Omega_m} \quad (3)$$

while the entropy at concentration x is given by the temperature-independent "ideal"expression:

$$S_{\text{ideal}}(x) = -R\,[x \ln x + (1-x)\ln(1-x)]. \quad (4)$$

While the real configurational entropy can be expected to depart significantly from the ideal expression when the composition is not close to that of the endmembers, the fact that the mixing is very endothermic implies that the thermodynamic analysis of the solid solution is only meaningful for x near 0 or 1. Our analysis will focus on these compositions, where the ideal expression for the configurational entropy is sensible. A similar approach has been followed before in the description of other metastable solid solutions, e.g. $Ce_{1-x}Zr_xO_2$ (Grau-Crespo et al., 2011) and $Ca_{1-x}Mg_x(PO_4)_6(OH)_2$ (Almora-Barrios et al., 2013). Having obtained the enthalpy and free energy of the solid solution, it is possible to evaluate the enthalpy of mixing:

$$\Delta H_{\text{mix}} = H[\text{Co}_x\text{Ca}_{1-x}\text{CO}_3] - (1-x)H[\text{CaCO}_3] - xH[\text{CoCO}_3] \quad (5)$$

which in principle can be compared with experimental calorimetric determinations, and the free energy of mixing:

$$\Delta G_{\text{mix}} = \Delta H_{\text{mix}} - TS_{\text{ideal}} \quad (6)$$

which can be used to determine the stability limits of the solid solution with respect to phase separation. Within this model, the enthalpy of mixing is the only contribution to the excess free energy (difference between the free energy of mixing and the ideal term $-TS_{\text{ideal}}$). Vibrational contributions to the mixing thermodynamics are not considered here, because they are typically small and, in comparison with the large mixing enthalpies in this system, their relative contributions will be minor. Also the pressure-volume contribution to the enthalpies are very small and can be ignored, so in the previous equations we use the DFT energies in place of the enthalpies. The other possible contributions to the errors in our model is the accuracy of these DFT energies, but these are obtained using standard and well-studied approximations, as discussed in detail below. We therefore think that our model gives a much better account of the thermodynamics of mixing in this solid solution than any model extracted from the observation of the compositions of either natural or synthetic samples.

2.2 Calculation of energies and geometries

The energies of different configurations of the mixed solid were evaluated by solving the periodic Schrödinger equation, using the density functional theory (DFT). All calculations were performed with the VASP code (Kresse and Furthmüller, 1996a, b), using the generalized gradient approximation (GGA) with the PBE exchange correlation functional (Perdew et al., 1996). In order to improve the DFT description of the highly localised *d* orbitals, we have employed the so-called GGA+U correction scheme, where we have used a Hubbard parameter U_{eff} = 6.1 eV, which is the value found for Co 3*d* by Wdowik and Parlinski (2007) to reproduce the experimental band gap of cobalt (II) oxide (CoO). All calculations involving Co(II) cations were performed allowing

spin polarization, as these cations formally have the electronic configuration $3d^7$ and therefore 3 unpaired electrons (S=3/2 in high-spin configurations). According to experiment, the magnetic moments in $CoCO_3$ are ordered antiferromagnetically at very low temperatures, but the low value of the Néel temperature (T_N=18.1 K) indicates that the coupling is very weak (Meshcheryakov, 2006). Therefore, the relative orientation of the Co(II) spin moments is not expected to have any significant effect on the calculated energies, and in this work we always use ferromagnetic orientations for computational convenience. A test calculation in pure $CoCO_3$ confirms that the energy difference between ferromagnetic and antiferromagnetic configurations is very small (less than 5 meV per formula unit). The interaction between the valence electrons and the core was described with the projected augmented wave (PAW) method (Blöchl, 1994) in the implementation of Kresse and Joubert (1999). The core levels up to 3*s* in Ca, 3*p* in Co, and 1*s* in C and in O were kept frozen in their atomic reference states. Due to the large size of the supercell, only the Γ point was used to sample the reciprocal space for the Brillouin zone integrations. The number of plane waves in VASP is controlled by a cutoff energy, in our case 520 eV, which is 30% higher than the standard value for the PAW potentials employed, in order to minimise the Pulay stress error and obtain accurate cell parameters. Each structure was fully relaxed to the equilibrium geometry using a conjugate gradients algorithm, which stops when the forces on the atoms are all less than 0.01 eV/Å. All the precision parameters in the calculations were tested to provide a level of convergence of the energies to within 5 meV per metal carbonate formula unit (1 meV per atom).

3. RESULTS AND DISCUSSION

3.1 Description of the end members

We first describe the results of our DFT calculations for the pure carbonates (Table 2). Both calcite ($CaCO_3$) and spherocobaltite ($CoCO_3$) have rhombohedral symmetry ($R\bar{3}c$ space group). We compare our cell parameters and coordinates with those obtained by Graf (1961) for both minerals using X-ray diffraction. The agreement is very good; the calculations slightly overestimate the cell parameters, but the deviations are small and similar for both minerals (~1.1% for *a*, and ~0.8% for *c*). Due to the smaller ionic radius of Co^{2+} compared to Ca^{2+}, the experimental unit cell volume of spherocobaltite is 76.4% of that of calcite. This volume ratio is accurately reproduced by the calculations, which gives 76.5%. In the pure hexagonal carbonates, the ionic coordinates of the carbon and metal (M=Ca or Co) ions are fixed by the crystal symmetry to Wyckoff positions 6a and 6b, respectively, while the oxygen ions are in the 18e positions, which are completely determined by a single parameter x_O. This parameter, together with the cell parameters, determines the C-O and M-O distances, which again are only slightly and systematically overestimated by the calculations in comparison with experiment, as shown in Table 2.

Apart from the differences in cell parameters and ionic distances, the simulations should also be able to reproduce the compressibilities of the two end-members of the solid solution. Compressibility can be expected to play an important role in the energetics of site substitutions, especially when the distributed ions have significantly different radii, as is the case for Ca^{2+} and

Co^{2+}. Therefore, we have also compared the calculated variation of the cell volumes under pressure with experimental results (Zhang and Reeder, 1999), for both calcite and spherocobaltite (Fig. 2a). Our calculations show that spherocobaltite is less compressible than calcite, in agreement with experiment. This result is consistent with the general trend within metal carbonates, where the bulk modulus decreases with the ambient cell volume (Zhang and Reeder, 1999). The bulk moduli for both structures were obtained by fitting the calculated energy vs volume data using the equation (Murnaghan, 1944):

$$E(V) = E_0 + V_0 B_0 \left[\frac{1}{B_0'(B_0'-1)} \left(\frac{V_0}{V} \right)^{(B_0'-1)} + \frac{1}{B_0'} \frac{V}{V_0} - \frac{1}{B_0'-1} \right]. \quad (7)$$

The results are B=70 GPa for calcite and B=107 GPa for spherocobalite, and the fitted curves can be seen in Fig. 2b. The bulk modulus of spherocobaltite is ~14% below the experimental result (125 GPa), but still significantly higher than the bulk modulus of calcite, as expected. The calculated bulk modulus of calcite is very close to the experimental value (67 GPa).

3.2 Substitutions at low concentrations: solution energies

We now examine the energetic cost of substituting one Co for Ca in calcite, or one Ca for Co in spherocobaltite, at the most dilute concentration (molar fraction x=1/24=0.042) allowed by our supercell size. At this concentration, the interactions between impurities are very small, as they are ~10 Å apart in the *ab* plane, and even farther apart in the *c* direction. We define the solution energy of Co in calcite as:

$$W_{\mathrm{cal}}[\mathrm{Co}^{2+}] = E[\mathrm{Ca}_{23}\mathrm{Co}(\mathrm{CO}_3)_{24}] - \frac{23}{24} E[\mathrm{Ca}_{24}(\mathrm{CO}_3)_{24}] - \frac{1}{24} E[\mathrm{Co}_{24}(\mathrm{CO}_3)_{24}], \quad (8)$$

i.e., the energy required to substitute one Co ion (taken from spherocobaltite) into calcite. The calculated value is $W_{\mathrm{cal}}[Co^{2+}]$=24.1 kJ/mol, which is almost ten times larger than the thermal energy RT at room temperature (2.5 kJ/mol), thus indicating very low solubility.

We also calculate a solution energy of Ca^{2+} in spherocobaltite, using an equation analogous to (8), and we obtain $W_{\mathrm{sph}}[Ca^{2+}]$=42.9 kJ/mol, indicating even lower solubility at this end of the solid solution. The energetic cost of substituting Ca^{2+} in Co^{2+} sites is much higher than that of the inverse substitution, as expected based on the ionic radii of the two cations. This result confirms that the assymetry of the thermodynamic miscibility gap assumed by Glynn (2000) is in the wrong direction, and that natural abundances give a very poor indication of solubility limits in this system.

The very high solution energies are not surprising considering that the ionic radius of Co^{2+} is 26% smaller than the radius of Ca^{2+}. This difference in ionic radius is much larger than the value of 15% that is typically regarded as the maximum ion size difference for the occurrence of extensive substitutions of one ion type by another in a solid (Goldschmidt, 1937; Ringwood, 1955a, b).

For comparison, we have also calculated the solution energy of Co^{2+} in aragonite, the second most common polymorph of $CaCO_3$,

which has an orthorhombic structure. We obtained $W_{ara}[Co^{2+}]$=103 kJ mol^{-1}, which is nearly three times larger than the solution energy of Co^{2+} in calcite. This very high solution energy, which suggests that no cobalt will be incorporated in the aragonite bulk, is due to the difficulty for a small cation like Co^{2+} to fulfil the nine-fold coordination of the cation sites in the aragonite structure. In fact, pure cobalt carbonate with the aragonite structure does not occur and any Co/Ca substitution in aragonite will be limited to the surface.

3.3 Disordered solid solution

We now consider more extensive substitutions of cobalt for calcium in calcite. Although, according to the results presented above, the thermodynamic solubilities are very small, there is experimental evidence of the formation of $Ca_{1-x}Co_xCO_3$ solid solutions, both in nature (Glynn, 2000) and in precipitation experiments (Katsikopoulos et al., 2008a). The substitution of Co in Ca sites, up to x=0.33, was supported by X-ray diffraction measurements in the latter study. These solid solutions are clearly metastable with respect to phase separation. Therefore, we will not attempt to establish the equilibrium degree of ordering of the cations in the solid solution, and will instead consider the limits of full disorder (in this section) and complete order (in the following section).

Fig. 3 shows the enthalpies of mixing as a function of Co molar fraction x, as calculated using Eq. (5). In principle, enthalpies of mixing can be obtained experimentally using calorimetric methods, but data are not available for this system, due to the difficulty in obtaining single-phase $Ca_{1-x}Co_xCO_3$ solid solution samples. Our calculations show that the formation of the disordered solid solution from pure calcite and spherocobaltite is endothermic for all the compositions investigated. Although intermediate compositions were not considered due to the higher computational cost of evaluating the corresponding ensembles (and their unlikely occurrence due to the highly endothermic mixing), it is possible to fit the calculated data to an assymmetric curve in the form of a two-parameter Guggenheim polynomial:

$$\Delta H_{\mathrm{mix}} = x(1\text{-}x)[W_0 + W_1(2x\text{-}1)], \quad (9)$$

for which we obtain W_0=34.0 kJ/mol and W_1=7.7 kJ/mol. The assymetric character of our $\Delta H_{mix}(x)$ is given by the positive value of the parameter W_1. The energetic cost of doping calcite with Co^{2+} from spherocobaltite in the dilute limit is W_0-W_1=26.3 kJ/mol, which is very close to the solution energy calculated in the previous section using only one substitution at x=1/24 ($W_{cal}[Co^{2+}]$=24.1 kJ/mol). The cost of doping spherocobaltite with Ca^{2+} from calcite in the dilute limit is W_0+W_1=41.7 kJ/mol (similar to $W_{sph}[Ca^{2+}]$=42.9 kJ/mol).

We can use the calculated enthalpy of mixing to estimate the thermodynamic miscibility between the two carbonates. If we assume a sub-regular solution model as previously done by Katsikopoulos et al. (2008a), but using our thermodynamic parameters, we can write the excess free energy as equal to the mixing enthalpy:

$$\Delta G^{\mathrm{E}}(x) = \Delta H_{\mathrm{mix}}(x) = x(1\text{-}x)RT[a_0 + a_1(2x\text{-}1)], \quad (10)$$

where a_0=W_0/RT and a_1=W_1/RT are the dimensionless Guggenheim parameters, which are inversely proportional to temperature in

the sub-regular model (a_0=13.73 and a_1=3.11 at 298.15 K). The thermodynamic miscibility gap at any temperature is fully determined by the values of a_0 and a_1: the limits of the gap are the two points of common tangent of the free energy of mixing (Prieto, 2009):

$$\Delta G_{\mathrm{mix}}(x) = \Delta G^{\mathrm{E}}(x) - TS_{\mathrm{ideal}}. \quad (11)$$

In the special case of the regular solid solution (a_0>0, a_1=0), the two points of common tangent are simply the minima of $\Delta G_{\mathrm{mix}}(x)$ (assuming that a_0>2, otherwise there are no minima). We have numerically determined the points of common tangent for different temperatures, which defines the solvus of the solid solution (Fig. 4). From these calculations, we can see that the thermodynamic limits for both Co incorporation in calcite and Ca incorporation in spherocobaltite are very small at ambient temperature. Even at 600 K, the maximum amount of Co in calcite is 0.52 mol%, while the maximum amount of Ca in spherocobaltite is ~0.02 mol%. At higher temperatures the miscibility gaps becomes narrower, but the analysis at very high temperatures becomes meaningless because calcite typically decomposes at ~1000 K, while spherocobaltite decomposes at even lower temperatures (the precise decomposition temperatures and rates depends on CO_2 partial pressures, particle size and other factors (Beruto et al., 2004; Rodriguez-Navarro et al., 2009)). For comparison, we have also plotted the low-temperature solvus obtained from the thermodynamic parameters of Glynn (2000) (regular model at each end of the solid solution, with a_0=4.12 for Co in calcite and a_0=3.26 for Ca in spherocobaltite at T=298.15 K), which yields a much higher miscibility between the two carbonates, thus placing observed mineral compositions within the region of miscibility. Our results suggest that the mineral compositions quoted in that study correspond to solid solutions that are metastable with respect to phase separation.

Another mathematical construction of interest based on our free energy model is the spinodal (dashed line in Fig. 4), which is given by the inflection points of the mixing free energy (points where $\Delta G''_{\mathrm{mix}}(x) = 0$). In the region inside the spinodal, $\Delta G''_{\mathrm{mix}}(x) < 0$, which means that the solid solution is unstable with respect to small composition fluctuations. Therefore demixing from these compositions can occur via a continuous process involving compositional modulations within the crystal, a process that is only limited by the diffusivity of the ions in the lattice. In contrast, compositions in the region between the spinodal and the solvus (where $\Delta G''_{\mathrm{mix}}(x) > 0$) can only demix via the nucleation of a separate phase with a composition on the opposite side of the solvus line. This discontinuous process involves an activation barrier and is likely to be much slower than the spinodal decomposition (Putnis, 1992). Therefore, both from thermodynamic and kinetic points of view, solid solutions in the region within the spinodal are much more susceptible to demixing than those in the region between the spinodal and the solvus, and therefore they are also less likely to form in nature and in experiment (although not impossible: for example, such compositions can be achieved via super-fast cooling from high temperatures, and the decomposition process at low temperature could be almost permanently inhibited by large ion diffusion barriers (Putnis, 1992)). Based on our calculations, natural calcite minerals with high Co concentrations of up to 2.7 mol% are unstable to demixing, but are still outside the spinodal. However, the Co concentrations of up

to 33% reported in the ambient-temperature precipitation experiments by Katsikopoulos et al. (2008a) fall well within the spinodal region, while their X-Ray Diffraction measurements of the crystalline phase showed no evidence of composition modulation or any strong heterogeneity. We will argue below (in Section 3.5), based on the comparison of observed and expected variations of cell parameters with composition, that the high Co contents reported in that study might not be incorporated into the bulk solid solutions. On the other end of the solid solution, the maximum observed Ca content in mineral spherocobaltite (~7 mol%) is also within the spinodal at near ambient temperature, but in this case it is reasonable to assume that these minerals are formed at much higher temperatures, which can exist under hydrothermal conditions.

3.4 Ordering of cobalt impurities in (0001) layers

The occurrence of ordered structures in mixed calcite-structured carbonates is a common phenomenon. A well-known example is the dolomite structure ($Ca_{0.5}Mg_{0.5}CO_3$) where Ca and Mg order in alternate layers with (0001) orientation, i.e., perpendicular to the *c* axis. This trend is also reported for other rhombohedral carbonate solid solutions in which the substituting cation is smaller than Ca^{2+} (Capobianco et al., 1987). The mixed carbonate $Ca_{0.5}Mn_{0.5}CO_3$ also exists with a dolomite-type structure, as the mineral kutnahorite (Frondel and Bauer, 1955). Katsikopoulos et al. (2009) suggested that in $Ca_{1-x}Mn_xCO_3$ the interactions between the Mn impurities are attractive within the (0001) layers, but repulsive between layers. Atomistic simulations of the (Ca, Mn)CO_3 system have confirmed the energetic preference for Mn^{2+} ions to aggregate in (0001) layers (Vinograd et al., 2010; Wang et al., 2011).

We therefore now examine the energetics of Co ordering in calcite. A simple inspection of our results confirms that, for all compositions, the lowest-energy configuration in the ensemble is the one with the maximum level of aggregation of Co ions within (0001) layers, and the maximum distance between Co layers. For compositions x=1/6, 1/3, 1/2, 2/3 and 5/6, there are ideally ordered configurations that satisfy exactly these requirements (Fig. 5). In principle it is possible to have these ideally ordered configurations for any composition, using larger supercells. For example, we have created a perfectly ordered configuration with x=1/12 by using a 1x1x2 supercell of the hexagonal unit cell of calcite.

The enthalpy of mixing for the ordered solid solution can then be obtained by interpolating the results from these special configurations, including the x=1/12 point. The result is shown in Fig. 3, together with the curve for the disordered solution. As expected, the enthalpy of mixing is considerably lower for the ordered configurations than for the disordered solution (which is an average over all the configurations). The enthalpy of mixing with Co layering is fitted to a higher-order (n=4) Guggenheim polynomial to account for the complex variation with composition:

$$\Delta H_{\text{mix}} = x(1-x)\sum_{n=0}^{4} W_n (2x-1)^n \qquad (12)$$

and we obtained: W_0=1.66 kJ/mol, W_1=0 (fixed to force the minimum at x=1/2), W_2=33.41 kJ/mol, W_3=5.15 kJ/mol and W_4=-23.63

kJ/mol.

The lower enthalpy of mixing does not imply that $Co_xCa_{1-x}CO_3$ solid solutions will be preferentially ordered. The relative stabilities of ordered vs disordered solid solutions can only be elucidated by comparing their free energies. The configurational entropy of the ordered phases is zero, while the configurational entropy of the fully disordered solution is a function of x (equation 4). Therefore the region of stability of the ordered phase with respect to the disordered phase is determined by both composition and temperature. The condition G(order) < G(disorder) is only satisfied for temperatures below the "layering temperature":

$$T_{\text{layering}}(x) = \frac{\Delta H_{\text{mix}}(\text{disorder}) - \Delta H_{\text{mix}}(\text{order})}{S_{\text{ideal}}(x)} \tag{13}$$

which are plotted in the phase diagram of Fig. 4, together with the solvus and spinodal. At temperatures $T<T_{\text{layering}}$, the stabilization of the disordered solid solution due to the configurational entropy is not enough to overcome its less favourable enthalpy of mixing, and then cation ordering becomes more favourable than disorder.

However, it is important to note that ordered phases are *always* unstable with respect to demixing. This is the case because for the ordered phase the enthalpy of mixing is always positive, while there are no configurational entropy stabilization effects. Therefore, the conclusion here is that while the ordered phase is never stable thermodynamically, metastable solid solutions (inside the solvus) might occur with some partial ordering of Co and Ca, as there is a clear energetic driving force towards layering.

3.5 Variation of cell parameters with composition

Fig. 6a shows the calculated cell parameters as a function of composition, for both the ordered and the disordered solid solution, in comparison with the values obtained by X-ray diffraction (XRD) of the samples of Katsikopoulos et al. (2008a). The experimental values for the end-member $CoCO_3$ were taken from Pertlik (1986) because Katsikopoulos et al. could not obtain pure $CoCO_3$ via precipitation from aqueous solution. The calculated cell parameters are very similar for the ordered and the disordered solids, indicating that the cation distribution has very little effect on the cell geometry. However, there is a marked difference between the calculated and the experimental values, in particular for the c parameter, which is expected to be more sensitive to composition based on the difference between its values for calcite and spherocobaltite. The experimental measurements lead to a large positive excess volume:

$$V^{\text{E}} = V_{\text{ss}} - V_{\text{mm}} \tag{14}$$

i.e., a larger solid solution volume (V_{ss}) compared to the volume of the mechanical mixture of the two end-members:

$$V_{\text{mm}} = (1\text{-}x)V_{\text{cal}} + xV_{\text{sph}}\,, \tag{15}$$

while the calculated volumes vary almost linearly with composition, with only a very small negative excess volume (Fig. 6b).

The discrepancy between our calculations and the experimental report should not be attributed necessarily to inaccuracies

in the simulation model. Obviously, XRD measurements of the cell parameters are reliable. However, due to the limitations of the energy dispersive spectrometry (EDS) technique, the composition assumed in the experiments by Katsikopoulos et al. might not correspond to the actual composition of the formed $Ca_{1-x}Co_xCO_3$ solid solutions. The total precipitates in these experiments consisted of a mixture of phases, so the EDS composition analysis could have measured an attached Co-rich phase at the same time as the calcite-structured solid solution. Another possibility is that the surface of the solid, which is measured by the EDS, is enriched in Co with respect to the bulk solid solution. In either case, the lower Co content in the solid solution with respect to the measured sample would explain the slow variation of the measured solid solution cell volume with the sample composition. This explanation is also consistent with our previous thermodynamic analysis, showing that concentrations up to 33% are too high, falling within the spinodal decomposition region of the phase diagram.

3.6 Equilibrium of the solid solution-aqueous solution

We now discuss the effect of the strong non-ideality of the solid solution on the equilibrium with an aqueous solution of the same ions. We have calculated the equilibrium values of the distribution coefficient:

$$D = \frac{(\mathrm{Co/Ca})_{\mathrm{ss}}}{(\mathrm{Co/Ca})_{\mathrm{aq}}} = \frac{x/(1-x)}{[\mathrm{Co}^{2+}]_{\mathrm{aq}}/[\mathrm{Ca}^{2+}]_{\mathrm{aq}}} \tag{16}$$

i.e. the ratio between the Co/Ca ratios in the solid and in the aqueous solution. The equilibrium value:

$$D_{\mathrm{eq}}(x) = \frac{K_{\mathrm{cal}}\gamma_{\mathrm{cal}}(x)}{K_{\mathrm{sph}}\gamma_{\mathrm{sph}}(x)} \tag{17}$$

is determined by the solubilities (K_{cal} and K_{sph}) of the end-members in aqueous solution, and by the activity coefficients (γ_{cal} and γ_{sph} in the solid solution, which are functions of the solid composition x (Prieto, 2009). In a sub-regular solid solution with Guggenheim dimensionless parameters a_0 and a_1, the activity coefficients can be obtained from the equations (Redlich and Kister, 1948):

$$\ln\gamma_{\mathrm{sph}} = (1-x)^2\left[a_0 + a_1(4x-1)\right], \tag{18}$$

$$\ln\gamma_{\mathrm{cal}} = x^2\left[a_0 + a_1(4x-3)\right]. \tag{19}$$

For the numerical evaluations presented in this work, the solubility product constants of calcite and spherocobaltite at room temperature in aqueous solution are taken from the MINTEQ.V4.DAT database (Allison et al., 1991): $10^{-8.48}$ for calcite and $10^{-9.98}$ for spherocobaltite. However, it should be noted here that there are significant disparities in the literature about the solubility constant of spherocobaltite. For example, the CHEAQS database (Verweij, 2005) compiles a solubility product of $10^{-11.2}$ for this carbonate. This value would lead to different quantitative predictions in the portioning model, but the same qualitative behaviour, as discussed below.

The results are plotted in Fig. 7. In order to illustrate the effects of non-ideality and of the assymmetry in the mixing free energy, we have also plotted the equilibrium distribution coefficients for the ideal solution (a_0=a_1=0) and for the regular solution (a_0 as in the sub-regular solution, but a_1=0). In an ideal solid solution, the activity coefficients both equal 1, and the equilibrium distribution coefficient is simply equal to the ratio between the solubilities of the end members. The result is a constant value, D_{eq}(ideal)=32, for all compositions. This value would be ~16 times higher if the solubility of spherocobaltite was taken from the CHEAQS database, which would shift up the horizontal line describing the ideal behaviour. But in either case the qualitative picture is the same: since spherocobaltite is less soluble in water than calcite, in an ideal solid solution there would be a preferential partitioning of the Co atoms towards the solid phase (D_{eq}>1).

In the highly non-ideal but symmetric solid solution (regular model, with a_0=13.73 and a_1=0) the deviation from the ideal partitioning behaviour is considerable: the partitioning will now occur preferentially towards the aqueous phase at low Co contents in the solid, but towards the solid phase in Co-rich solid solutions. The corresponding curve vs x is a straight line in the logarithmic plot, although due to the very wide miscibility gap at ambient temperature, it is only meaningful to examine the equilibrium distribution coefficients near the endmembers. The strong non-ideality has the general effect of making the concentration of impurities in each endmember solid very small, regardless of the aqueous solution composition. Even in equilibrium with a very Co-rich aqueous solution, calcite will have a very low level of substitutional cobalt impurities. On the other end, even in equilibrium with very low Co/Ca ratios, spherocobaltite will incorporate very small amounts of Ca as substitutional impurities in the bulk.

Finally, the effect of the asymmetry in the mixing free energy (sub-regular model with a_0=13.73 and a_1=3.11) leads to some convexity in the logarithmic plot of D_{eq}, in such a way that the partitioning of Co ions between calcite and an aqueous solution occurs less preferentially towards the aqueous phase (more Co is incorporated in the solid phase for a given composition of the aqueous phase). On the other compositional end, less Ca is incorporated in spherocobaltite in equilibrium, in comparison with the behaviour of the regular solid solution. This is the expected result considering that Ca incorporation in spherocobaltite is more endothermic than Co incorporation in calcite. We can illustrate these effects with some numbers: in equilibrium with an aqueous solution with a Co/Ca ratio of 1, calcite would take up ~0.1% (1000 ppm) Co^{2+} ions in substitutional positions, while spherocobaltite would take up less than 0.01 ppm of Ca^{2+} ions. The asymmetry between the behaviour of the endmembers of the solid solution in terms of equilibrium ion exchange with the aqueous solution arises not only from the asymmetry in the mixing enthalpy, but also from the difference in solubility between spherocobaltite and calcite (an effect that can be described even when the regular solution model is employed, as seen above). Both effects contribute to make substitutional mixing even more difficult in the pure Co limit than in the pure Ca limit.

It is important to emphasize that, due to the uncertainties in the solubility data, our theoretical predictions should only be taken as qualitative: numerical discrepancies of one order of magnitude or more can be expected for the calculated equilibrium distribution coefficients if different databases are used to extract the values of the solubility product of spherocobaltite.

Unfortunately, experimental information cannot be used here for benchmarking, because measurements of the distribution coefficient of Co in calcite have only been carried out under non-equilibrium conditions. Lorens (1981) reported values between 2 and 8, which are much higher than those obtained from our calculations (regardless of the database used for the solubilities), but these measured values were found to vary significantly with the precipitation rate of calcite, confirming the presence of strong non-equilibrium effects.

4. Conclusions

We have conducted a computer simulation study of the thermodynamics of mixing between calcite ($CaCO_3$) and spherocobaltite ($CoCO_3$). Our main conclusions are summarized below:

i) The mixing of calcite and spherocobaltite is a highly endothermic process, as expected from the relatively large difference in the ionic radii of Co^{2+} and Ca^{2+}, but in contrast with previous estimations based on the natural abundance of $Ca_{1-x}Co_xCO_3$ minerals and on the measured composition of synthetic samples.

ii) The mixing enthalpy of the disordered solution can be described by a two-parameter Guggenheim polynomial with W_0=34.0 kJ/mol and W_1=7.7 kJ/mol. The positive value of W_1 indicates that the incorporation of Ca from calcite into spherocobaltite takes more energy than the incorporation of Co from spherocobaltite in calcite. The consideration of a sub-regular solid solution model with these parameters leads to the conclusion that calcite and spherocobaltite are not thermodynamically miscible at any significant level at ambient temperature, which suggest that observed solid solutions in nature and experiment are metastable with respect to phase separation.

iii) The lowest-energy configuration for each composition is the one with the maximum level of aggregation of Co ions within (0001) layers, and simultaneously the maximum distance between Co layers. This is consistent with a model of effective attractive interactions between equal ions within a layer, and effective repulsive interactions between layers of the same ion.

iv) The enthalpy of mixing for the ordered phase is always lower than the enthalpy of mixing for the disordered phase. Therefore, at low temperatures ordering is thermodynamically favourable over disorder. However, the ordered phases are always unstable with respect to phase separation, regardless of composition. The metastable formation of fully ordered phases is unlikely; layering can only be expected to occur to a limited extent, accompanied by significant levels of partial disorder.

v) The variation of cell parameters with composition is predicted to be linear in the disordered solid solution, with only a very small (and negative) excess volume. Cation ordering in (0001) layers would not alter this linearity to any significant extent. This result contrasts with a previous report of a very positive excess volume measured in synthetic samples with up to 33 mol% of Co (Katsikopoulos et al., 2008a). We have argued here that the Co content in the solid solution might have been overestimated in that study due to the limitations of the energy dispersive spectrometry (EDS) technique. This would be consistent with the very low miscibility predicted by our calculations, and would also explain the almost constant value of the *c* parameter with composition in

the experimental study. Further experimental research on these Co-bearing phases formed under conditions of high supersaturation would be welcomed to verify our conclusions.

vi) The strong non-ideality of this solid solution has an important effect on the solid solution / aqueous solution thermodynamic partitioning: the equilibrium level of substitutional impurities in the endmember solids is always low, regardless of the composition of the aqueous solution. Thus, even in equilibrium with a very Co-rich aqueous solution, calcite is predicted to have a very low level of cobalt impurities, which is unfortunate as it means that Co/Ca substitution in calcite is not an effective way to immobilize Co(II) cations in solution. On the other hand, our results also mean that if spherocobaltite could be formed (which is admittedly difficult due to competition from other cobalt-bearing phases), almost perfect immobilization of the Co^{2+} ions would be achieved as there would be negligible Ca^{2+}/Co^{2+} ion exchange with aqueous solutions.

ACKNOWLEDGMENTS

This work was supported by the FPI program of the Spanish Ministry of Economy and Competitiveness (Grant CGL2010-20134-CO2-02). We thank Prof. Manuel Prieto for useful discussions.

Table 1. Total number of configurations (*W*) and number of symmetrically inequivalent configurations (*M*) for each composition $Co_xCa_{1-x}CO_3$ in a 2×2×1 supercell (A and B stand for either Ca or Co).

Cell composition	*x or 1-x*	*W*	*M*
$A_{24}(CO_3)_{24}$	0	1	1
$A_{23}B(CO_3)_{24}$	0.042	24	1
$A_{22}B_2(CO_3)_{24}$	0.083	276	7
$A_{21}B_3(CO_3)_{24}$	0.125	2024	20
$A_{20}B_4(CO_3)_{24}$	0.167	10626	102

Table 2. Calculated crystal geometries and bulk moduli of calcite and spherocobaltite, in comparison with experiment.

Property	*$CaCO_3$ (calcite)*		*$CoCO_3$ (spherocobaltite)*	
	Calculated	*Experiment*	*Calculated*	*Experiment*
a (Å)	5.047	4.990[a]	4.712	4.658[a]
c (Å)	17.193	17.062[a]	15.083	14.958[a]
x_O	0.2575	0.2578[a]	0.2755	0.276[a]
d[C-O] (Å)	1.300	1.286[a]	1.298	1.286[a]
d[M-O] (Å)	2.382	2.357[a]	2.133	2.109[a]
B (GPa)	70	67[b]	107	125[b]

[a] Graf, 1961; [b] Zhang and Reeder, 1999.

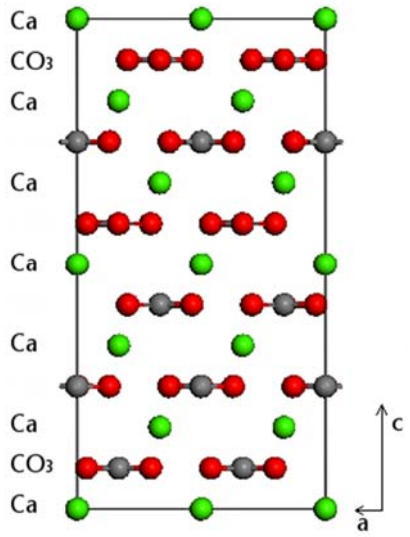

Fig. 1. The structure of calcite in a 2×2×1 supercell (Ca = green, C = grey, O = red).

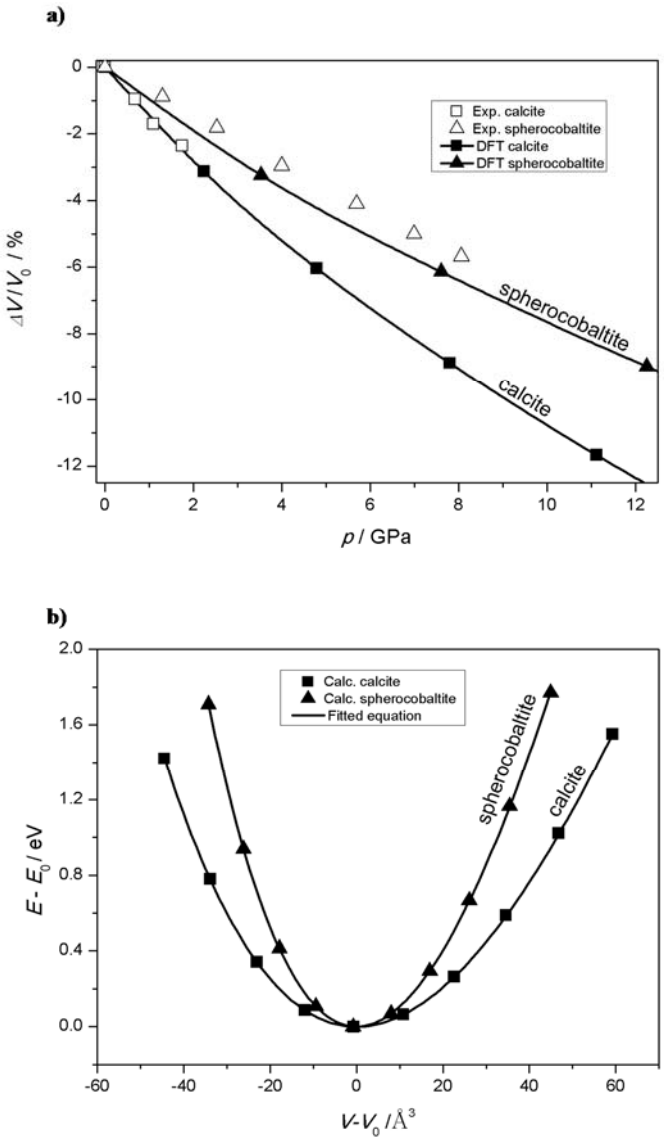

Fig. 2. a) Calculated variation of the cell volumes with pressure for calcite and spherocobaltite, in comparison with experiment (Zhang and Reeder, 1999). b) Fitting of the calculated energy-volume points using a Murnaghan equation of state.

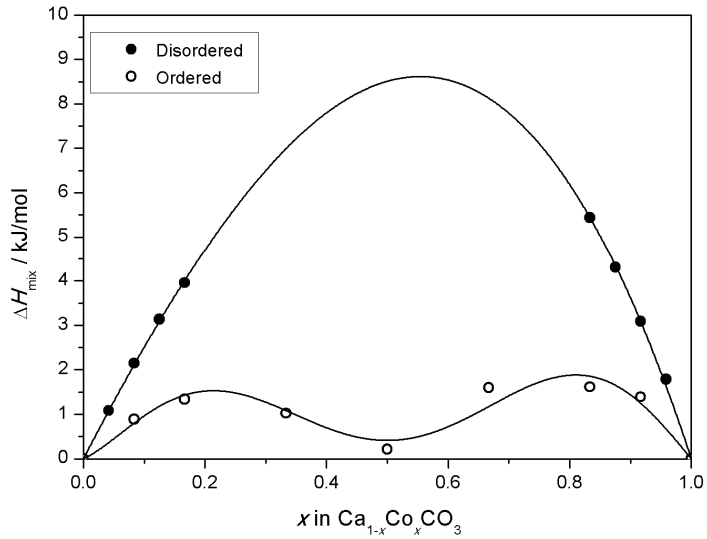

Fig. 3. Calculated mixing enthalpies for the $Co_xCa_{1-x}CO_3$ solid solution in the full-order and full-disorder limits.

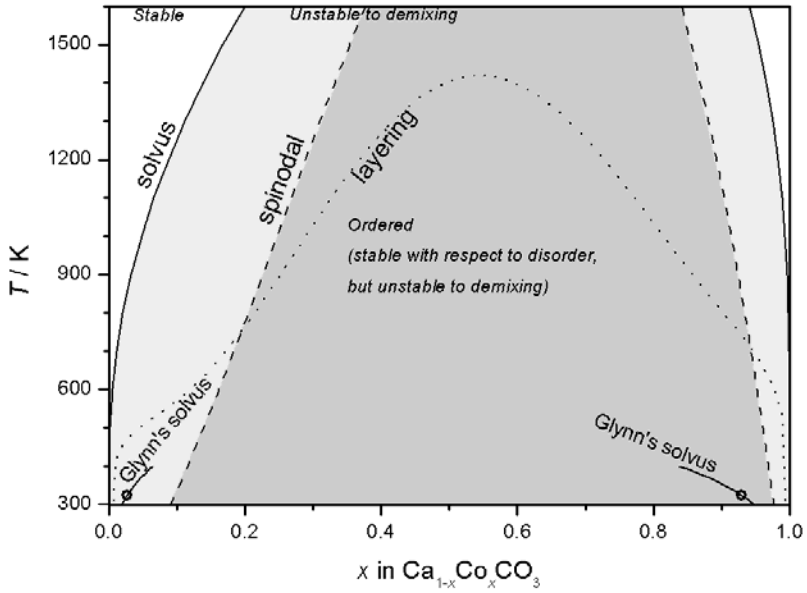

Fig. 4. Calculated solvus, spinodal and layering temperatures in the $Co_xCa_{1-x}CO_3$ solid solution.

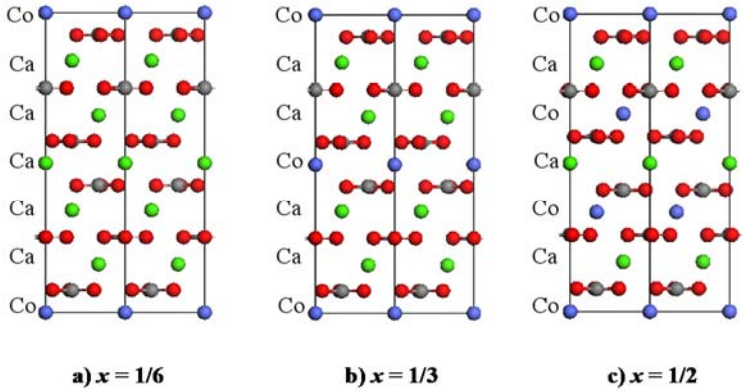

Fig. 5. Lowest-energy configurations of $Ca_{1-x}Co_xCO_3$ calculated for x=1/6, x=1/3 and x=1/2. The lowest-energy configurations for x>1/2 can be obtained from those with composition 1-x by swapping the Co and Ca positions (Ca = green, Co = blue, C = grey, O = red).

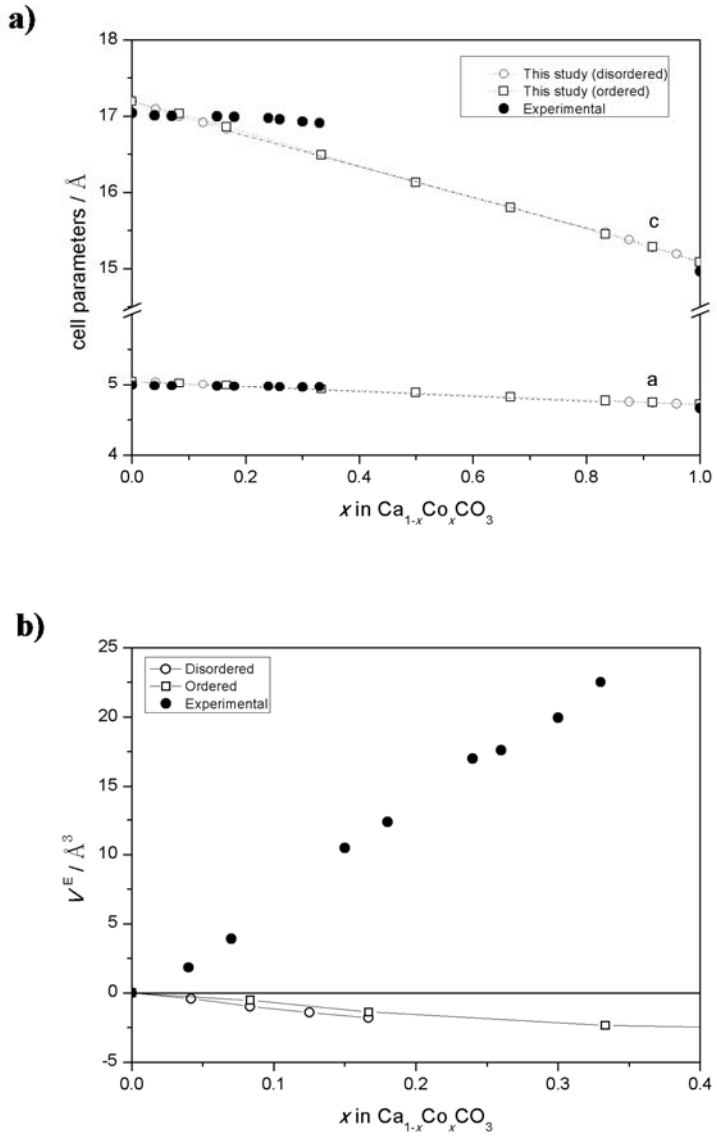

Fig. 6. a) Variation of the lattice parameters of $Co_xCa_{1-x}CO_3$ as a function of composition, in comparison with experiment (Katsikopoulos et al. 2008a). b) Variation of the excess volume as a function of composition in the Ca-rich member, contrasted to experimental results.

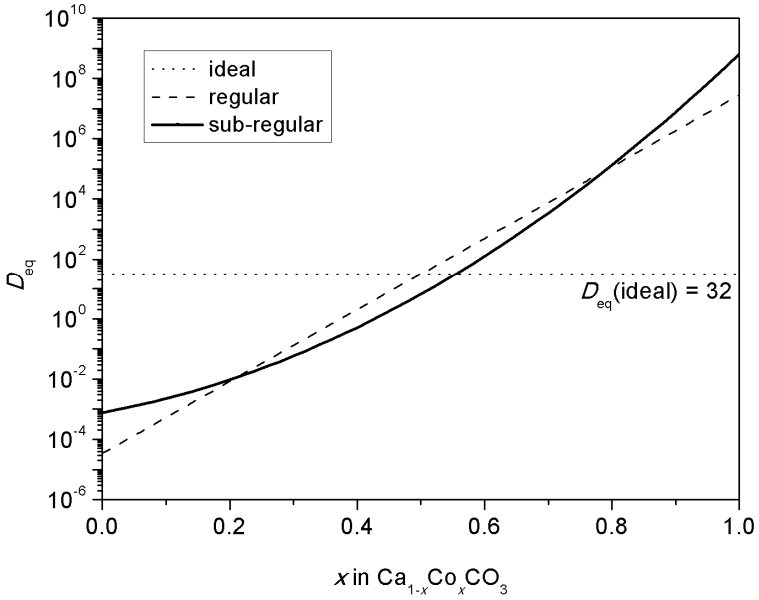

Fig. 7. Equilibrium aqueous-solid distribution coefficient for the $Co_xCa_{1-x}CO_3$ solid solution as a function of the solid composition. The sub-regular model parameters (a_0=13.73, a_1=3.11) are those obtained from DFT calculations; the regular (a_0=13.73, a_1=0) and ideal (a_0=a_1=0) lines are also plotted for comparison.

References

Allison, J.D., Brown, D.S., Novo-Gradac, K.J., 1991. MINTEQA2, a geochemical assessment model for environmental systems. Report EPA/600/3-91/0-21, U.S.Environmental Protection Agency, Athens, Georgia.

Almora-Barrios, N., Grau-Crespo, R., de Leeuw, N.H., 2013. A computational study of magnesium incorporation in the bulk and surfaces of hydroxyapatite. *Langmuir* **29**, 5851-5856.

Anthony, J.W., Bideaux, R.A., Bladh, K.W., Nichols, M.C., 2003. *Handbook of Mineralogy: Borates, Carbonates, Sulfates* (Vol. V). Mineral Data Publishing, Tucson. 813 pp.

ATSDR, 2004. Toxicological profile for cobalt. U.S. Department of Health and Human Services, Public Health Service, Atlanta.

Barceloux, D.G., 1999. Cobalt. *Clinical Toxicology* **37**, 201-216.

Benny, S., Grau-Crespo, R., de Leeuw, N.H., 2009. A theoretical investigation of α-Fe_2O_3–Cr_2O_3 solid solutions. *Physical Chemistry Chemical Physics* **11**, 808-815.

Beruto, D.T., Searcy, A.W., Kim, M.G., 2004. Microstructure, kinetic, structure, thermodynamic analysis for calcite decomposition: free-surface and powder bed experiments. *Thermochimica Acta* **424**, 99-109.

Blöchl, P.E., 1994. Projector augmented-wave method. *Physical Review B* **50**, 17953-17979.

Braybrook, A.L., Heywood, B.R., Jackson, R.A., Pitt, K., 2002. Parallel computational and experimental studies of the morphological modification of calcium carbonate by cobalt. *Journal of Crystal Growth* **243**, 336-344.

Capobianco, C., Burton, B.P., Davidson, P.M., Navrotsky, A., 1987. Structural and calorimetric studies of order-disorder in $CdMg(CO_3)_2$. *Journal of Solid State Chemistry* **71**, 214-223.

Davis, K.J., Dove, P.M., De Yoreo, J.J., 2000. The role of Mg^{2+} as an impurity in calcite growth. *Science* **290**, 1134-1137.

De Leeuw, N.H., Parker, S.C., 2000. Modeling absorption and segregation of magnesium and cadmium ions to calcite surfaces: Introducing $MgCO_3$ and $CdCO_3$ potential models. *The Journal of Chemical Physics* **112**, 4326-4333.

Fisler, D.K., Gale, J.D., Cygan, R.T., 2000. A shell model for the simulation of rhombohedral carbonate minerals and their point defects. *American Mineralogist* **85**, 217-224.

Frondel, C., Bauer, L.H., 1955. Kutnahorite - a Manganese Dolomite, Camn(Co3)2. *American Mineralogist* **40**, 748-760.

Glynn, P., 2000. Solid-solution solubilities and thermodynamics: sulfates, carbonates and halides. *Reviews in Mineralogy and Geochemistry* **40**, 481-511.

Goldschmidt, V.M., 1937. The principles of distribution of chemical elements in minerals and rocks *Journal of the Chemical Society Faraday Trans.*, 655-673.

Graf, D.L., 1961. Crystallographic tables for the rhombohedral carbonates. *American Mineralogist* **46**, 1283-1316.

Grau-Crespo, R., Al-Baitai, A.Y., Saadoune, I., De Leeuw, N.H., 2010. Vacancy ordering and electronic structure of γ-Fe_2O_3 (maghemite): a theoretical investigation. *Journal of Physics: Condensed Matter* **22**, 255401.

Grau-Crespo, R., de Leeuw, N.H., Hamad, S., Waghmare, U.V., 2011. Phase separation and surface segregation in ceria–zirconia solid solutions. *Proceedings of the Royal Society A: Mathematical, Physical and Engineering Science* **467**, 1925-1938.

Grau-Crespo, R., Hamad, S., Catlow, C.R.A., De Leeuw, N.H., 2007. Symmetry-adapted configurational modelling of fractional site occupancy in solids. *Journal of Physics: Condensed Matter* **19**, 256201.

Grau-Crespo, R., Smith, K.C., Fisher, T.S., De Leeuw, N.H., Waghmare, U.V., 2009. Thermodynamics of hydrogen vacancies in MgH_2 from first-principles calculations and grand-canonical statistical mechanics. *Physical Review B* **80**, 174117

Haider, S., Grau-Crespo, R., Devey, A.J., de Leeuw, N.H., 2012. Cation distribution and mixing thermodynamics in Fe/Ni thiospinels. *Geochimica et Cosmochimica Acta* **88**, 275-282.

Hildebrand, J.H., 1936. The Solubility of Non-Electrolytes; Reinhold: New York.

IARC, 1991. Chlorinated drinking-water; chlorination by-products; some other halogenated compounds; cobalt and cobalt compounds, *IARC Monographs on the Evaluation of Carcinogenic Risks to Humans*. World Health Organization, International Agency for Research on Cancer. , Lyon.

Katsikopoulos, D., Fernández-González, Á., Prieto, A.C., Prieto, M., 2008a. Co-crystallization of Co (II) with calcite: Implications for the mobility of cobalt in aqueous environments. *Chemical Geology* **254**, 87-100.

Katsikopoulos, D., Fernández-González, Á., Prieto, M., 2008b. Crystallization of the (Cd, Ca)CO_3 solid solution in double diffusion systems: the partitioning behaviour of Cd^{2+} in calcite at different supersaturation rates. *Mineralogical Magazine* **72**, 433-436.

Katsikopoulos, D., Fernández-González, Á., Prieto, M., 2009. Precipitation and mixing properties of the "disordered" (Mn,Ca)CO_3 solid solution. *Geochimica et Cosmochimica Acta* **73**, 6147-6161.

Kim, J.H., Gibb, H.J., Howe, P.D., Sheffer, M., 2006. *Cobalt and Inorganic Cobalt Compounds*. Concise International Chemical Assessment Document. World health organization.

Kresse, G., Furthmüller, J., 1996a. Efficiency of ab-initio total energy calculations for metals and semiconductors using a plane-wave basis set. *Computational Materials Science* **6**, 15-50.

Kresse, G., Furthmüller, J., 1996b. Efficient iterative schemes for ab initio total-energy calculations using a plane-wave basis set. *Physical Review B* **54**, 11169–11186.

Kresse, G., Joubert, D., 1999. From ultrasoft pseudopotentials to the projector augmented-wave method. *Physical Review B* **59**, 1758-1175.

Lorens, R.B., 1981. Sr, Cd, Mn and Co distribution coefficients in calcite as a function of calcite precipitation rate. *Geochimica et Cosmochimica Acta* **45**, 553-561.

McLean, D., 1957. *Grain boundaries in metals*. Clarendon, Oxford.

Meshcheryakov, V.F., 2006. Magnetization of the canted antiferromagnetic $CoCO_3$ in Abragam-Pryce approximation. *Journal of Magnetism and Magnetic Materials* **300**, e395-e398.

Meyer, H.J., 1984. The influence of impurities on the growth rate of calcite. *Journal of Crystal Growth* **66**, 639-646.

Murnaghan, F., 1944. The compressibility of media under extreme pressures. *Proceedings of the National Academy of Sciences of the United States of America* **30**, 244-247.

Noguera, C., Fritz, B., Clément, A., Amal, Y., 2010. Simulation of the nucleation and growth of binary solid solutions in aqueous solutions. *Chemical Geology* **269**, 89-99.

Perdew, J.P., Burke, K., Ernzerhof, M., 1996. Generalized gradient approximation made simple. *Physical Review Letters* **77**, 3865-3868.

Pertlik, F., 1986. Structures of hydrothermally synthesized cobalt (II) carbonate and nickel (II) carbonate. *Acta Crystallographica Section C: Crystal Structure Communications* **42**, 4-5.

Prieto, M., 2009. Thermodynamics of solid solution-aqueous solution systems. *Reviews in Mineralogy and Geochemistry* **70**, 47-85.

Prieto, M., Fernández-González, Á., Putnis, A., Fernández-Díaz, L., 1997. Nucleation, growth, and zoning phenomena in crystallizing (Ba, Sr) CO_3, Ba (SO_4, CrO4),(Ba, Sr) SO_4, and (Cd, Ca) CO_3 solid solutions from aqueous solutions. *Geochimica et Cosmochimica Acta* **61**, 3383-3397.

Putnis, A., 1992. *An introduction to mineral sciences*. Cambridge University Press.

Redlich, O., Kister, A.T., 1948. Algebraic Representation of Thermodynamic Properties and the Classification of Solutions. *Industrial & Engineering Chemistry* **40**, 345-348.

Ringwood, A., 1955a. The principles governing trace-element behaviour during magmatic crystallization: Part II. The role of complexx formation. *Geochimica et cosmochimica acta* **7**, 242-254.

Ringwood, A., 1955b. The principles governing trace element distribution during magmatic crystallization Part I: The influence of electronegativity. *Geochimica et cosmochimica acta* **7**, 189-202.

Rodriguez-Navarro, C., Ruiz-Agudo, E., Luque, A., Rodriguez-Navarro, A.B., Ortega-Huertas, M., 2009. Thermal decomposition of calcite: Mechanisms of formation and textural evolution of CaO nanocrystals. *American Mineralogist* **94**, 578-593.

Ruiz-Hernandez, S.E., Grau-Crespo, R., Ruiz-Salvador, A.R., De Leeuw, N.H., 2010. Thermochemistry of strontium incorporation in aragonite from atomistic simulations. *Geochimica et Cosmochimica Acta* **74**, 1320-1328.

Ruiz-Salvador, A.R., Grau-Crespo, R., Gray, A.E., Lewis, D.W., 2013. Aluminium distribution in ZSM-5 revisited: The role of Al–Al interactions. *Journal of Solid State Chemistry* **198**, 330-336.

Sánchez-Pastor, N., Gigler, A.M., Cruz, J.A., Park, S.-H., Jordan, G., Fernández-Díaz, L., 2011. Growth of calcium carbonate in the presence of Cr (VI). *Crystal Growth & Design* **11**, 3081-3089.

Seminovski, Y., Palacios, P., Wahnon, P., Grau-Crespo, R., 2012. Band gap control via tuning of inversion degree in $CdIn_2S_4$. *Applied Physics Letters* **100**, 102112.

Shannon, R., 1976. Revised effective ionic radii and systematic studies of interatomic distances in halides and chalcogenides. *Acta Crystallographica Section A* **32**, 751-767.

Smith, I., Carson, B.L., 1981. *Trace metals in the environment vol 6. Cobalt an apraisal of environmental exposure* Ann Arbor Science Publishers Inc, Ann Arbor

Smith, K.C., Fisher, T.S., Waghmare, U.V., Grau-Crespo, R., 2010. Dopant-vacancy binding effects in Li-doped magnesium hydride. *Physical Review B* **82**, 134109.

Veizer, J., 1983. Trace elements and isotopes in sedimentary carbonates. *Reviews in Mineralogy and Geochemistry* **11**, 265-299.

Verweij, W., 2005. Chemical Equilibria in Aquatic Systems—CHEAQS-PC Calculating Program. http://home.tiscali.nl/cheaqs/index.html.

Vinograd, V.L., Burton, B.P., Gale, J.D., Allan, N.L., Winkler, B., 2007. Activity–composition relations in the system $CaCO_3$–$MgCO_3$ predicted from static structure energy calculations and Monte Carlo simulations. *Geochimica et Cosmochimica Acta* **71**, 974-983.

Vinograd, V.L., Paulsen, N., Winkler, B., van de Walle, A., 2010. Thermodynamics of mixing in the ternary rhombohedral carbonate solid solution, (CaxMgy, Mn1-x-y)CO3, from atomistic simulations. *Calphad-Computer Coupling of Phase Diagrams and Thermochemistry* **34**, 113-119.

Wada, N., Yamashita, K., Umegaki, T., 1995. Effects of divalent cations upon nucleation, growth and transformation of calcium carbonate polymorphs under conditions of double diffusion. *Journal of Crystal Growth* **148**, 297-304.

Wang, Q., Grau-Crespo, R., de Leeuw, N.H., 2011. Mixing Thermodynamics of the Calcite-Structured (Mn, Ca)CO_3 Solid Solution: A Computer Simulation Study. *The Journal of Physical Chemistry B* **115**, 13854-13861.

Wdowik, U.D., Parlinski, K., 2007. Lattice dynamics of CoO from first principles. *Physical Review B* **75**, 104306.

Zhang, J., Reeder, R.J., 1999. Comparative compressibilities of calcite-structure carbonates: Deviations from empirical relations. *American Mineralogist* **84**, 861-870.